

Journal of Nanophotonics

Nanophotonics.SPIEDigitalLibrary.org

Design of polymer multilayer heterostructure broadband reflector for the near-infrared using genetic algorithm

Xiang Cheng
Weimin Yang
Chengyou Lin
Yumei Ding
Zhiwei Jiao

SPIE.

Xiang Cheng, Weimin Yang, Chengyou Lin, Yumei Ding, Zhiwei Jiao, "Design of polymer multilayer heterostructure broadband reflector for the near-infrared using genetic algorithm," *J. Nanophoton.* 11(3), 036021 (2017), doi: 10.1117/1.JNP.11.036021.

Design of polymer multilayer heterostructure broadband reflector for the near-infrared using genetic algorithm

Xiang Cheng,^a Weimin Yang,^{a,b} Chengyou Lin,^c Yumei Ding,^a and Zhiwei Jiao^{a,*}

^aBeijing University of Chemical Technology, College of Mechanical and Electrical Engineering, Beijing, China

^bBeijing University of Chemical Technology, Beijing Advanced Innovation Center for Soft Matter Science and Engineering, Beijing, China

^cBeijing University of Chemical Technology, College of Science, Beijing, China

Abstract. A broadband reflector for the near-infrared (NIR) was designed using a multilayer heterostructure consisting of several quarter-wave stacks (QWSs), which were composed of polymethyl methacrylate (PMMA) and polyethylene terephthalate (PET) films. Taking the solar power density as the target and using the Bragg wavelength of each QWS as the variable, the genetic algorithm was applied to look for the optimal multilayer heterostructure for broadband NIR reflection. As high as 99.46% total energy reflectivity in the short-wavelength NIR region (780 to 1100 nm) and 89.56% total energy transmissivity in the visible light region (380 to 780 nm) were realized by a multilayer heterostructure consisting of six quarter-wave PMMA/PET stacks, which can be easily fabricated based on the micronano multilayer coextrusion technology. The designed structure possesses good stability, and its total energy reflectivity is not sensitive to the incident angle of light. The proposed broadband NIR reflector can be applied to buildings as energy-saving films. © 2017 Society of Photo-Optical Instrumentation Engineers (SPIE) [DOI: [10.1117/1.JNP.11.036021](https://doi.org/10.1117/1.JNP.11.036021)]

Keywords: broadband reflector; near-infrared; quarter-wave stacks; polymethyl methacrylate/polyethylene terephthalate; energy-saving.

Paper 17038 received Mar. 30, 2017; accepted for publication Aug. 31, 2017; published online Sep. 21, 2017.

1 Introduction

Global climate change results from the construction of expensive building environments, such as air-conditioning systems.¹ The near-infrared (NIR) spectrum in the solar spectrum is one of the main causes for the rise of indoor temperatures in buildings. Therefore, improving the NIR reflectivity of a building, which can reduce the indoor temperature and avoid the use of expensive building environments, has become a primary method for dealing with such environmental problems.² Therefore, some experts have proposed cool materials, such as a masonry paint,³ selective coated glazing,⁴ transparent conductors,⁵ and nanopowder,⁶ but all of these materials suffer from low visible transmittance. To obtain a better performance, energy-saving glasses were widely studied.^{7–10} Compared with energy-saving glasses, energy-saving films exhibit outstanding advantages, such as low cost, high stability, and good durability.¹¹ The energy-saving films can be prepared by the following methods: ion-beam sputtering,¹² magnetron sputtering,^{13–15} coevaporation,^{16,17} and pulsed laser deposition.¹⁸ Variable materials with different refractive indices have also been used in films to obtain a better energy-saving effect.^{19–21} However, the improvements of these approaches are limited because of the high refractive index

*Address all correspondence to: Zhiwei Jiao, E-mail: jjaozw@mail.buct.edu.cn

contrast materials used in energy-saving films, making them unsuitable for large-scale application and industrialization.

In this paper, a broadband NIR reflector with a polymer multilayer heterostructure was designed using the genetic algorithm (GA). The multilayer heterostructure consists of several quarter-wave stacks (QWSs) composed of polymethyl methacrylate (PMMA) and polyethylene terephthalate (PET) films with low refractive index contrast. By optimizing the Bragg wavelength of each PMMA/PET QWS, high reflectivity in the NIR region and high transmissivity in the visible light region were realized by a single polymer multilayer heterostructure. In addition, the feasibility of preparing such a polymer multilayer heterostructure based on the micro-nano multilayer coextrusion technology was discussed.

2 Modeling of Optical Thin Film

2.1 Polymer Multilayer Heterostructure

To design a broadband NIR reflector, a multilayer heterostructure consisting of several PMMA/PET QWSs was proposed, as shown in Fig. 1. For each PMMA/PET QWS, high-reflection can be realized near its Bragg wavelength λ_B ($B = 1 - k$), which is related to the thicknesses of the PMMA and PET layers ($n_{\text{PMMA}}d_{\text{PMMA}} \cos \theta_{\text{PMMA}} = n_{\text{PET}}d_{\text{PET}} \cos \theta_{\text{PET}} = \lambda_B/4$).

2.2 Transfer-Matrix Method

To calculate the reflectivity R of the proposed polymer multilayer heterostructure, the transfer matrix method²² was used

$$M = \begin{bmatrix} A & B \\ C & D \end{bmatrix} = \sum_{j=1}^m \begin{bmatrix} \cos \delta_j & i \sin \delta_j / \eta_j \\ i \eta_j \sin \delta_j & \cos \delta_j \end{bmatrix}, \quad (1)$$

$$r = \frac{\eta_0(A + B\eta_{N+1}) - C - D\eta_{N+1}}{\eta_0(A + B\eta_{N+1}) + C + D\eta_{N+1}}, \quad (2)$$

$$R = r \cdot r^*, \quad (3)$$

where M is the characteristic matrix of the multilayer heterostructure and its matrix elements are A , B , C , and D . δ_i and η_i are the phase factor and the optical admittance for each layer, respectively. $\delta_i = 2\pi n_i d_i \cos \theta_i / \lambda$ ($i = 1 - N$) in which n_i and d_i represent the refractive index and the layer thickness of each layer, respectively. λ is the wavelength of incident light, and θ_i is the refraction angle of light in each layer. $\eta_i = n_i \cos \theta_i$ or $\eta_i = n_i / \cos \theta_i$ ($i = 1 - N$) applies to s- or p-polarized light. N is the layer number of the multilayer heterostructure, and $N = 2S \times k$ for the proposed multilayer heterostructure. η_0 and η_i are the optical admittance for incident and emergent media, respectively. r is the spectral complex amplitude reflection coefficient.

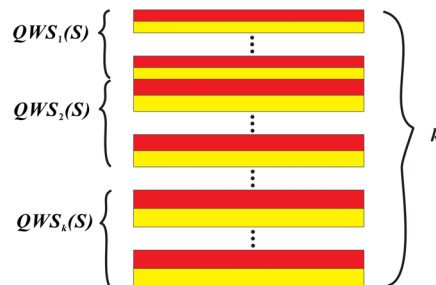


Fig. 1 Schematic diagram of the multilayer heterostructure consisting of k PMMA/PET QWSs (each stack contains S PMMA/PET bilayers).

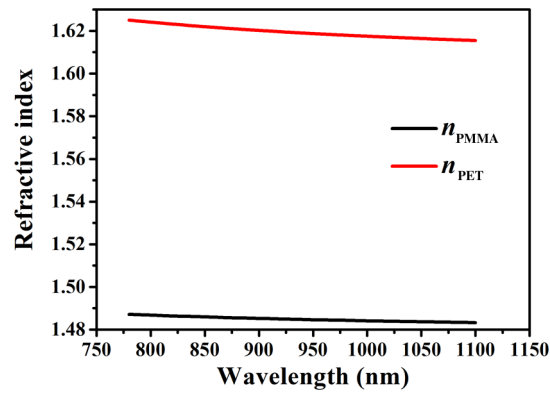


Fig. 2 Dispersion curves of PMMA and PET in the NIR region.

In our simulation, only normal incidence of light was considered ($\theta_0 = 0$). $S = 64$ was used to guarantee nearly 100% reflection in the Bragg wavelength for each PMMA/PET QWS. In addition to improve the simulation accuracy, the dispersion effects of PMMA and PET were considered in our calculation, as shown in Fig. 2.^{23,24}

2.3 Genetic Algorithm

For the design of the broadband NIR reflector with high reflectivity, the GA, which has been recognized as a great optimization method and excellent global searching tool for multilayer design, was used in our simulation. By choosing the appropriate merit function (MF) in the GA, one can control the optimization direction of the GA and finally obtain the optimal multilayer. In our simulation, the MF is defined as the total energy reflectivity R_{total} as follows:

$$\text{MF} = R_{\text{total}} = \frac{I_o(\lambda_B)}{I_i(\lambda_B)} = \frac{\sum_{j=1}^m I(\lambda_j) \cdot R(\lambda_j)}{\sum_{j=1}^m I(\lambda_j)}, \quad (4)$$

where I_o or I_i is the total output or input energy of the solar source (Fig. 3) and they are both the functions of Bragg wavelength λ_B . $I(\lambda_j)$ is the energy of incident light λ_j and $R(\lambda_j)$ is the reflectivity of the broadband NIR reflector at the wavelength λ_j . By maximizing the MF in Eq. (4), one can obtain the optimal wavelength λ_B for the maximum reflection in the desired spectral range, which is the short-wavelength NIR region (780 to 1100 nm) in our study.

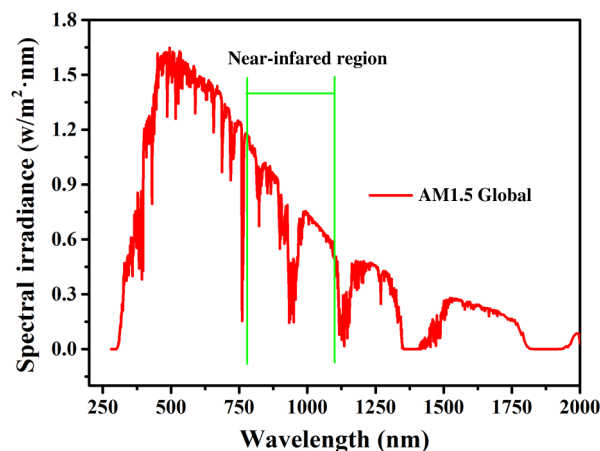


Fig. 3 The NIR region in the AM1.5 solar spectrum.

3 Numerical Simulation

3.1 Reflection Effects of Different Quarter-Wave Stacks

The reflectivity of the designed polymer multilayer heterostructure with only one QWS ($k = 1$) is shown in Fig. 4(a), and the bandwidth of the high-reflection region is only 40 nm (840 to 880 nm), making it difficult to completely cover the short-wavelength NIR region (780 to 1100 nm) and leading to low total energy reflectivity R_{total} [see Fig. 4(b)].

Fortunately, R_{total} in the short-wavelength NIR region (780 to 1100 nm) can be improved with the increase of the number of QWSs (k), as shown in Fig. 5. However, when k becomes larger than 6, R_{total} remains the same value since nearly 100% R_{total} is obtained.

3.2 Optimal Polymer Multilayer Heterostructure

Considering the processing accuracy of the micronano multilayer coextrusion technology, the number of QWSs in the PMMA/PET multilayer heterostructure should be as small as possible. Therefore, the optimal number k is 6 according to the results shown in Fig. 5. Figure 6 shows the reflectivity and the output spectrum for the designed polymer multilayer heterostructure with six QWSs ($k = 6$). The designed multilayer film shows 99.63% R_{total} in the desired spectral region (780 to 1100 nm). In addition, the total energy transmissivity of the designed multilayer heterostructure in the visible light region is 89.54%.

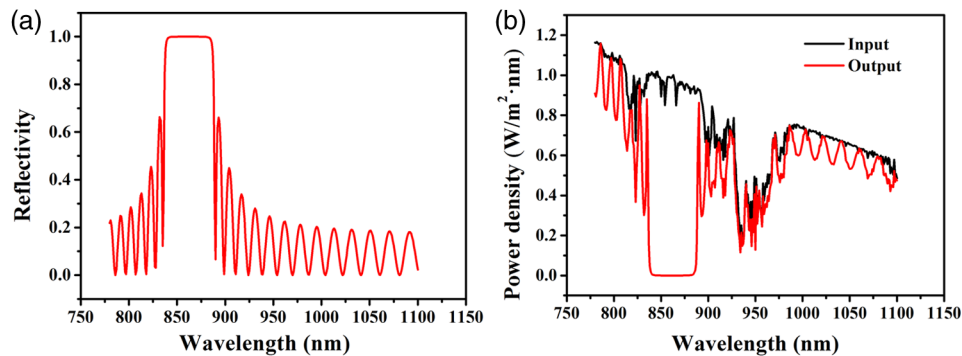


Fig. 4 (a) The reflectivity and (b) the output spectrum (including incident solar source for comparison) for the designed polymer multilayer heterostructure with only one QWS ($k = 1$).

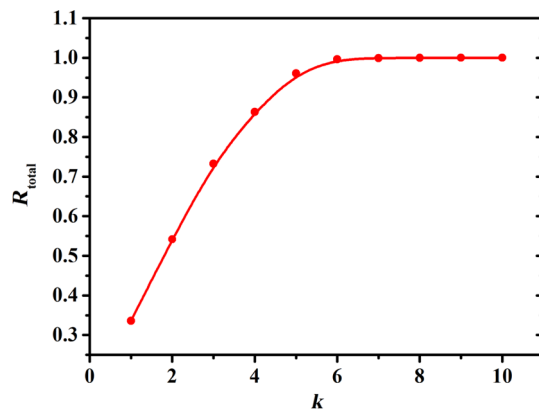


Fig. 5 Dependence of the optimal NIR (780 to 1100 nm) spectral reflectance (R_{total}) on the number of QWSs (k) in the PMMA/PET multilayer heterostructure.

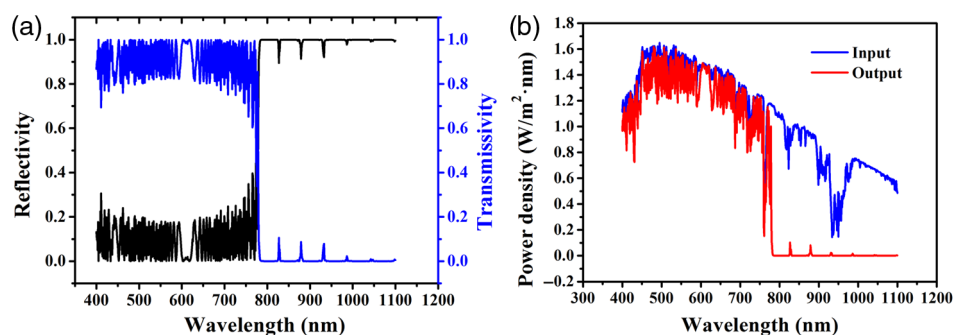


Fig. 6 (a) The reflectivity and (b) the output spectrum (including incident solar source for comparison) for the designed polymer multilayer heterostructure with six QWSs ($k = 6$).

Table 1 The thicknesses of PMMA and PET layers in the optimal multilayer heterostructure.

Stacks	PMMA (nm)	PET (nm)	PMMA/PET (nm)
QWS ₁	143.4973	131.6489	275.1462
QWS ₂	134.9460	123.8036	258.7496
QWS ₃	152.2038	139.6365	291.8404
QWS ₄	161.6752	148.3259	310.0011
QWS ₅	180.9545	166.0133	346.9679
QWS ₆	170.9342	156.8204	327.7546

Due to the dispersion effects of PMMA and PET, the thickness ratio of the PMMA and PET layers in each QWS is not the same for six QWSs. However, the thickness ratio of the PMMA and PET layers in each QWS should be consistent in the micronano multilayer coextrusion technology. Since the thickness ratio of PMMA to PET in each QWS is around 1.09, we set 1.09 as the uniform thickness ratio and revised the thicknesses of the PET layers in each QWS, as shown in Table 1. The revised structure still shows high total energy reflectivity (99.46%) in the short-wavelength NIR region (780 to 1100 nm) and high total energy transmissivity (89.56%) in the visible light region (380 to 780 nm).

3.3 Preparing Polymer Multilayer Heterostructure

Multilayer structures can be manufactured by the micronano multilayer coextrusion technology based on torsion lamination (US 9079346B2). Compared with the method using overpass lamination (US 5094788) of the 3M Company, the method using torsion lamination can be used to ensure good smoothness of the films.²⁵⁻²⁷ In the preparation process as shown in Fig. 7, PMMA and PET are extruded through two extruders and converged through the converger to the PMMA/PET double-layer structure of the melt with a certain thickness ratio. When passing through the laminator, the double-layer melt is first divided into four tracks in the transverse direction. The four-channel double-layer melt is twisted at 90 deg and extended to the width before cutting in the width direction, thus forming the periodic structure with $2 \times 4 = 8$ layers. Three four-channel laminators are connected in series, and a multilayer heterostructure with $2 \times 4^3 = 128$ layers is formed. Then a six-channel laminator is used. The ratio that the last laminator (the six-channel laminator) divides the melt into is equal to the thickness ratio of PMMA or PET in six QWSs (1.063:1:1.128:1.198:1.341:1.267), according to Table 1. Then the multilayer heterostructure is formed by the extrusion die and stretching machines to keep the ratio constant and achieve the specific thickness. The specific thickness is the sum of thicknesses of all layers (nearly 116 μm), according to Table 1.

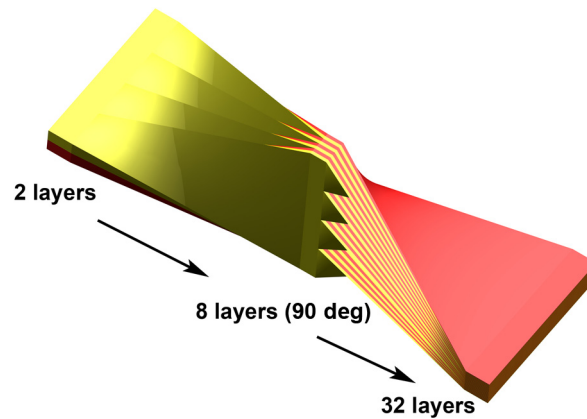


Fig. 7 The micronano multilayer coextrusion technology based on torsion lamination.

3.4 Influence of Thickness Error on the Optimal Near-Infrared (780 to 1100 nm) Spectral Reflectance

Due to machining error of inner flow channels and shrinkage of the two polymers, a thickness error occurs in the preparation process. Compared with a machining error, the shrinkage of the two polymers causes much larger errors. According to the shrinkage ratios of the two materials, the thickness error is $<5\%$. It is assumed that there is an error in the thicknesses of the designed polymer multilayer heterostructure with six QWSs ($k = 6$). The thickness of each layer fluctuates around the ideal thickness d_i , and the thickness fluctuation range is $(d_i \pm \Delta d)$, in which Δd is a parameter that characterizes thickness error or nonuniform error. The maximum value of Δd is nearly 10 nm. Then the thickness error is randomly added to change the thickness of each layer ($d_i \pm \Delta d$). The results of the NIR (780 to 1100 nm) spectral reflectance R_{total} were examined with 500 random changes, as shown in Fig. 8.

As shown in Fig. 8, though the thickness fluctuation is considered, the range of the NIR (780 to 1100 nm) spectral reflectance R_{total} is up to $98.43\% \pm 0.43\%$, which shows a small deviation from the ideal value (99.46%). Therefore, our designed polymer multilayer heterostructure is not sensitive to thickness error of the micronano multilayer coextrusion technology, which means the designed structure has good stability.

3.5 Influence of Incident Angle of Light on the Optimal Near-Infrared (780 to 1100 nm) Spectral Reflectance

The calculations in the previous sections are done under normal incidence of light; the influence of the incident angle of light on the optimal NIR (780 to 1100 nm) spectral reflectance is shown in Fig. 9. In the NIR band with high energy (780 to 870 nm), a photonic bandgap can be achieved by the designed polymer multilayer heterostructure with six QWSs, as shown in Fig. 9(a).

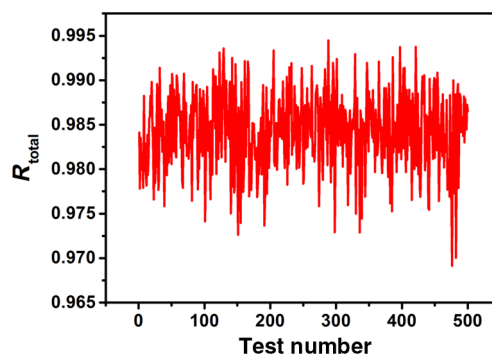


Fig. 8 The NIR (780 to 1100 nm) spectral reflectance (R_{total}) with 500 random changes.

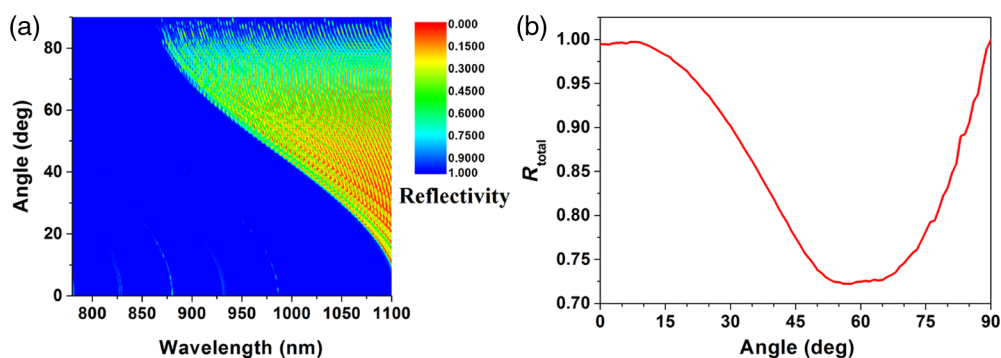


Fig. 9 (a) The reflectivity R_{total} of the designed structure calculated by simulation based on the incident angle and the wavelength and (b) dependence of the reflectance R_{total} in the NIR spectrum (780 to 1100 nm) on the incident angle.

When the incident angle increases from 0 deg to 90 deg, the reflectivity of the designed structure in the band of 780 to 870 nm keeps nearly 100%. Thus, the reflectance R_{total} of the designed structure in the NIR region (780 to 1100 nm) is always high (above 70%). The results indicate that the designed polymer multilayer heterostructure with high reflectivity for the NIR region (780 to 1100 nm) is not sensitive to the incident angle, compared with another sensitive filters.²⁸

4 Conclusion

A broadband reflector with a polymer multilayer heterostructure for the NIR region (780 to 1100 nm) is designed using the GA. The optimal polymer multilayer heterostructure consists of six QWSs composed of PMMA and PET films with low refractive index contrast and exhibits 99.46% total energy reflectivity in the short-wavelength NIR region (780 to 1100 nm). The designed polymer multilayer heterostructure possesses good stability, and its total energy reflectivity is not sensitive to the incident angle of light. This type of multilayer film can be easily fabricated by the micronano multilayer coextrusion technology based on torsion lamination for large-scale application and industrialization.

Acknowledgments

This work was supported by the National Key R&D Program of China (No. 2016YFB0302000), the Natural Science Foundation of Beijing Municipality (No. 2162033), and the National Natural Science Foundation of China (No. 51576012).

References

1. C. Lamnatou and D. Chemisana, "Solar radiation manipulations and their role in greenhouse claddings: Fresnel lenses, NIR- and UV-blocking materials," *Renewable Sustainable Energy Rev.* **18**(2), 271–287 (2013).
2. N. Deforest et al., "Regional performance targets for transparent near-infrared switching electrochromic window glazings," *Build. Environ.* **61**, 160–168 (2013).
3. M. Zinzi, "Characterisation and assessment of near infrared reflective paintings for building facade applications," *Energy Build.* **114**, 206–213 (2016).
4. S. C. Kim, J. H. Yoon, and H. M. Lee, "Comparative experimental study on heating and cooling energy performance of spectrally selective glazing," *Sol. Energy* **145**, 78–79 (2017).
5. C. G. Granqvist, "Transparent conductors as solar energy materials: a panoramic review," *Sol. Energy Mater. Sol. Cells* **91**, 1529–1598 (2007).
6. R. Yang et al., "Synthesis, characterization and thermal performance of Fe/N co-doped MgTiO₃ as a novel high near-infrared reflective pigment," *Sol. Energy Mater. Sol. Cells* **160**, 307–318 (2017).

7. C. L. Huang, C. C. Ho, and Y. B. Chen, "Development of an energy-saving glass using two-dimensional periodic nano-structures," *Energy Build.* **86**(1197), 589–594 (2015).
8. H. Ye, X. Meng, and B. Xu, "Theoretical discussions of perfect window, ideal near infrared solar spectrum regulating window and current thermochromic window," *Energy Build.* **49**(2), 164–172 (2012).
9. S. Hoffmann, E. S. Lee, and C. Clavero, "Examination of the technical potential of near-infrared switching thermochromic windows for commercial building applications," *Sol. Energy Mater. Sol. Cells* **123**(123), 65–80 (2014).
10. N. Deforest et al., "United States energy and CO₂ savings potential from deployment of near-infrared electrochromic window glazings," *Build. Environ.* **89**, 107–117 (2015).
11. E. Stulz et al., "Efficient NIR light blockage with matrix embedded silver nanoprism thin films for energy saving window coating," *J. Mater. Chem. C* **4**(8), 1584–1588 (2016).
12. L. J. Meng, V. Teixeira, and M. P. D. Santos, "Effect of the deposition rate on ITO thin film properties prepared by ion beam assisted deposition (IBAD) technique," *Phys. Status Solidi A* **207**(7), 1538–1542 (2010).
13. M. C. Wang et al., "All-solid-state electrochromic device integrated with near-IR blocking layer for image sensor and energy-saving glass application," in *Int. Workshop on Active-Matrix Flatpanel Displays and Devices* (2016).
14. J. Chavez-Galan and R. Almanza, "Solar filters based on iron oxides used as efficient windows for energy savings," *Sol. Energy* **81**(1), 13–19 (2007).
15. J. Zheng, S. Bao, and P. Jin, "TiO₂(R)/VO₂(M)/TiO₂(A) multilayer film as smart window: combination of energy-saving, antifogging and self-cleaning functions," *Nano Energy* **11**, 136–145 (2015).
16. T. U. Ryu et al., "Optical, mechanical and thermal properties of MgF₂-ZnS and MgF₂Ta₂O₅ composite thin films deposited by coevaporation," *Opt. Eng.* **39**(12), 3207–3213 (2000).
17. W. Zhong et al., "Synthesis of CuS nanoplate-containing PDMS film with excellent near-infrared shielding properties," *RSC Adv.* **6**(23), 18881–18890 (2016).
18. L. Gong et al., "Highly transparent conductive and near-infrared reflective ZnO:Al thin films," *Vacuum* **84**(7), 947–952 (2010).
19. C. C. Lee, C. J. Tang, and J. Y. Wu, "Rugate filter made with composite thin films by ion-beam sputtering," *Appl. Opt.* **45**(7), 1333–1337 (2006).
20. T. Yang et al., "Double-layer anti-reflection coating containing a nanoporous anodic aluminum oxide layer for GaAs solar cells," *Opt. Express* **21**(15), 18207–18215 (2013).
21. Y. Shi et al., "Nanopyramids and rear-located Ag nanoparticles for broad spectrum absorption enhancement in thin-film solar cells," *Opt. Express* **22**(17), 20473–20480 (2014).
22. M. S. Islam, "Analytical modeling of organic solar cells including monomolecular recombination and carrier generation calculated by optical transfer matrix method," *Org. Electron.* **41**, 143–156 (2017).
23. J. F. Elman et al., "Characterization of biaxially-stretched plastic films by generalized ellipsometry," *Thin Solid Films* **313**(97), 814–818 (1998).
24. G. Beadie et al., "Refractive index measurements of poly(methyl methacrylate) (PMMA) from 0.4 – 1.6 μm," *Appl. Opt.* **54**(31), F139 (2015).
25. C. Li et al., "Properties of polypropylene/multiwall carbon nanotube composite films prepared by microlayer extrusion," *J. Plast. Film Sheeting* **33**(2), 191–206 (2017).
26. L. Xiong et al., "Plasticizer migration from micro-layered flexible poly (vinyl chloride) films prepared by multi-layer co-extrusion technology," *J. Plast. Film Sheeting* **32**(4), 402–418 (2016).
27. M. Shi et al., "Interfacial diffusion and bonding in multilayer polymer films: a molecular dynamics simulation," *J. Phys. Chem. B* **120**(37), 10018–10029 (2016).
28. D. M. Nguyen, D. Lee, and J. Rho, "Control of light absorbance using plasmonic grating based perfect absorber at visible and near-infrared wavelengths," *Sci. Rep.* **7**(1), 2611 (2017).

Xiang Cheng obtained his bachelor's degree from Beijing University of Chemical Technology in 2012. Since 2014, he has been a combined master's–doctoral student and a teaching assistant at Beijing University of Chemical Technology. He works on soft robots, plastic cars, and

micronano multilayer coextrusion devices. He is also interested in optical thin films and tunable-focus lenses based on electroactive polymers.

Weimin Yang received his PhD in chemical process equipment from Beijing University of Chemical Technology in 1998. From October 2000 to September 2002, he was a postdoctoral fellow at Polymer Processing Yokoi Lab, the University of Tokyo, Japan. He is also a distinguished professor of Chang Jiang Scholars Program, China Ministry of Education. His research interests are polymer processing and advanced manufacture technology, mainly focusing on micronano multilayer coextrusion, plastics precision molding, nanofiber electrospinning, etc.

Chengyou Lin received his PhD in physics from Beijing Normal University, China in 2013. From September 2009 to August 2011, he was a visiting student at the Department of Electrical Engineering and Computer Sciences, University of California, Berkeley, USA. He is currently working as a lecturer in the College of Science, Beijing University of Chemical Technology, China. His research interests include surface plasmon resonance technology and thin-film optics.

Yumei Ding received her master's degree from Beijing University of Chemical Technology in 1990. She is an associate professor at Beijing University of Chemical Technology. She is currently actively involved in design and fabrication of energy-saving films as part of the Natural Science Foundation of Beijing. Her current research interests include micronano multilayer coextrusion, nanofiber electrospinning, and optical thin films.

Zhiwei Jiao received his PhD from Beijing University of Chemical Technology in 2012. He is an associate professor at Beijing University of Chemical Technology. He is currently actively involved in high-performance plastic films as part of the National Key R&D Program of China. His research interests include micronano multilayer coextrusion, three-dimensional printing, plastics precision molding, and optical thin films.